Determination of the electronic structure of bilayer graphene from infrared spectroscopy results

L. M. Zhang, Z. Q. Li, D. N. Basov, and M. M. Fogler
University of California San Diego, 9500 Gilman Drive, La Jolla, California 92093

Z. Hao and M. C. Martin
Advanced Light Source Division, Lawrence Berkeley National Laboratory, Berkeley, California 94720

(Dated: August 23, 2008)

We present an experimental study of the infrared conductivity, transmission, and reflection of a gated bilayer graphene and their theoretical analysis within the Slonczewski-Weiss-McClure (SWMc) model. The infrared response is shown to be governed by the interplay of the interband and the intraband transitions among the four bands of the bilayer. The position of the main conductivity peak at the charge neutrality point is determined by the interlayer tunneling frequency. The shift of this peak as a function of the gate voltage gives information about less known parameters of the SWMc model, in particular, those responsible for the electron-hole and sublattice asymmetries. These parameter values are in a fair agreement with recent electronic structure calculations for the bilayer graphene but different from the commonly cited estimates for the bulk graphite.

PACS numbers: 81.05.Uw, 78.30.Na, 78.20.Bh

I. INTRODUCTION

Since a monolayer graphene was isolated a few years ago,[1,2] ultrathin carbon systems have attracted tremendous attention.[3] Their electron properties are quite unique. Monolayer graphene has a vanishing Fermi point at the Brillouin zone corner and low energy quasiparticles with a linear spectrum, $\varepsilon(\mathbf{k}) = \pm v|\mathbf{k}|$, which obey a massless Dirac equation. Here $\mathbf{k}$ is the deviation of the crystal momentum from the Brillouin zone corner (K point), $v = (3/2)\gamma_0 a/\hbar$ is the quasiparticle velocity, γ_0 is the nearest-neighbor hopping parameter, and $a = 1.42\,\text{Å}$ is the carbon-carbon distance. Graphene is the basic building block of other types of carbon materials. Indeed, the first calculation of its band structure by Wallace[4] was motivated by his studies of graphite. Extending that work, Slonczewski and Weiss,[5] McClure,[5,6] and others[7] have developed the now commonly used Slonczewski-Weiss-McClure (SWMc) model for the low-energy electron properties of graphite. This model, which is equivalent to a tight-binding model with seven parameters, has proven to be a very useful analytical tool. It permitted theoretical calculations of a vast number of properties of graphite, including its diamagnetic susceptibility, de Haas-van Alfven effect, magnetooptical response, cyclotron resonance, and so on. These properties were actively studied experimentally until the late 70's and lead to accurate estimates of the principal SWMc parameters, γ_0 through γ_3. Still, it proved challenging to unambigously determine the remaining three SWMc constants γ_4, γ_5, and Δ, which are measured in tens of meV. For illustration, in Table I we list inequivalent parameter sets from the latest original sources, Refs. 8 and 9. Subsequently, the issue was further confounded by numerous misprints in reference books and reviews.[10]. The density-functional theory calculations,[11–13] which normally have accuracy of $\sim 0.1\,\text{eV}$ for quasiparticle dispersion, have not yet settled this discrepancy.

In view of the reinvigorated interest to graphene, it has become an important question to obtain the SWMc constants for a few layer graphene and also to compare them with those for bulk graphite. Thus, a significant difference between the graphite and a graphene bilayer was recently reported, based on the analysis of Raman scattering.[14] Several *ab initio* calculations of these parameters for the bilayer have also been done.[15–19] Unfortunately, they have not explicitly discussed the uncertain SWMc parameters.

The bilayer is a system intermediate between graphene and bulk graphite. Its lattice structure (for the case of the Bernal or AB stacking) is illustrated in Fig. 1(a). The corresponding band structure,[21,22] shown in Fig. 1(b), consists of four bands. These bands arise from splitting and hybridization of the Dirac cones of the individual layers by the interlayer hopping matrix element γ_1 and by the electrostatic potential difference V between the two layers.[23,24] The latter can be controlled experimentally by varying the voltage V_g of a nearby metallic gate[25,26] or by doping.[27] This degree of tunability makes the bilayer graphene an extremely interesting material for both fundamental study and applications.

In this paper we show that γ_1, $v_4 \equiv \gamma_4/\gamma_0$, and Δ

TABLE I: The SWMc parameters according to previous and present work. The numbers in parentheses indicate the reported accuracy of the trailing decimal places. The "Exp" and "DFT" stand for experiment and density functional theory, respectively.

SWMc	Graphene bilayer			Graphite, early work				Graphite, recent work	
Parameter	Pres. work	Exp[a]	DFT[b]	Exp[c]	Exp[d]	DFT[e]	DFT[f]	Exp[g]	DFT[h]
γ_0	3.0(3)[i]	2.9	2.6	3.16(5)	3.2	2.92	2.598(15)		
γ_1	0.40(1)	0.30	0.3	0.39(1)	0.397	0.27	0.364(20)		
γ_2	0.0[j]	0.0[j]	0.0[j]	-0.020(2)	-0.0202	-0.022	-0.014(8)		
γ_3		0.10	0.3	0.315(15)	0.29	0.27	0.319(20)		
γ_4	0.15(4)	0.30		0.044(24)	0.132	0.27	0.177(25)		
γ_5	0.0[j]	0.0[j]	0.0[j]	0.038(5)	0.0098	0.27	0.036(13)		
Δ	0.020(5)		0.01[k]	-0.008(2)	0.0221	0.0079	-0.026(10)	<0.01[l]	-0.037[m]

[a] L. M. Malard *et al.*, Phys. Rev. B **76**, 201401 (2007).[14]
[b] H. Min, B. R. Sahu, S. K. Banerjee, and A. H. MacDonald, Phys. Rev. B **75**, 155115 (2007).[18]
[c] M. S. Dresselhaus and G. Dresselhaus, Adv. Phys. **30**, 139 (1981).[8]
[d] R. O. Dillon, I. L. Spain, and J. W. McClure, J. Phys. Chem. Solids **38**, 635 (1977).[9]
[e] Tatar and Rabii, Phys. Rev. B **25**, 4126 (1982).[11]
[f] J.-C. Charlier, X. Gonze, and J.-P. Michenaud, Phys. Rev. B **43**, 4579 (1991).[12]
[g] M. Orlita *et al.*, Phys. Rev. Lett. **100**, 136403 (2008).[20]
[h] A. Grüneis *et al.*, Phys. Rev. Lett. **100**, 037601 (2008).[13]
[i] This value of γ_0 is assumed based on results in literature.
[j] Irrelevant in the bilayer.
[k] Our estimate based on digitizing band dispersion graphs published in Refs. 16–19.
[l] Absolute value only.
[m] The negative sign is required for consistency with the conventional definition[6] of Δ.

can be *directly* extracted from the dynamical condictivity measured in zero magnetic field. This is in contrast to the bulk graphite where determination of the SWMc constants was never straightforward and almost invariably required the use of strong magnetic fields.

The dynamical conductivity $\sigma(\Omega)$ is determined by the six possible transitions among the four bands, see Fig. 1(c). They have energies of the order of a few 10^{-1} eV, which is in the infrared optical range. Recently, experimental measurements of the infrared response of the bilayers have been carried out by our[28] and other[29,30] groups. Below we identify and explain the key findings of these experiments based on how different combinations of the interband transitions are either activated or suppressed by the Pauli exclusion principle. Our theory enables us to reach a quantitative agreement with the experiment using γ_0, γ_1, and γ_4, and Δ as adjustable parameters. The values of these parameters that give the best fit are given in the second column of Table I. Note that the next-nearest layer hopping parameters γ_2 and γ_5 are irrelevant for the bilayer. The parameter γ_3 cannot be reliably estimated from these particular experiments because they are largely insensitive to it in the range of carrier concentrations suitable for our analysis.

Previous theoretical studies of the optical conductivity of bilayer graphene[21,22,31–33] used a simplified model in which only γ_0 and γ_1 were taken into account. This model successfully explains the major features of $\sigma(\Omega)$ as well as its dependence on the gate voltage V_g, and we qualitatively summarize it as follows. Conduction and valence bands are symmetric. In the absence of the electrostatic potential difference V between the layers the two conduction (valence) bands have the same shape and are shifted by γ_1. Except the range of very small momenta k, their shape remain nearly identical even in the presence of a finite V. As a result, there is a high optical density of states for transitions between the two pairs of bands at frequency $\gamma_1/\hbar$, which gives rise to a sharp peak in the real part of the conductivity $\mathrm{Re}\,\sigma(\Omega)$ at $\Omega = \gamma_1/\hbar \approx 3200\,\mathrm{cm}^{-1}$ (using $\gamma_1 = 0.40\,\mathrm{eV}$). Other transitions give more gradually varying contributions to $\mathrm{Re}\,\sigma(\Omega)$, eventually leading to the asymptotic "universal" value[21,22,31–33] $\sigma = e^2/2\hbar$ at high frequency (which is twice the value for the monolayer[34]). Finally, in real graphene systems the conductivity features are never sharp because of a finite lifetime due to, e.g., disorder scattering. This broadens the peaks and can also merge together several features that are close in energy, see Fig. 2.

Our recent infrared experiments[28] as well as measurements by another group[30] have largely confirmed this picture but also found features that cannot be explained within this simple model. In particular, the conductivity peaks on the electron and the hole sides are displaced in energy from γ_1 by about $0.1\gamma_1$ in opposite directions. [Electron and hole doping is identified with, respectively, positive and negative $\delta V = V_g - V_{\mathrm{CN}}$, where V_{CN} is the gate voltage at which the bilayer is tuned to the charge-neutrality (CN) point.]

In order to investigate the origin of these features in this paper we carry out a combined experimental-theoretical study of the infrared response of a bilayer graphene. We attribute the observed electron-hole asymmetry to the effect of γ_4 and Δ. We find that including

these parameters is essential for a more accurate discussion of $\sigma(\Omega)$ of the bilayer. Besides differences in the optical response, γ_4 and Δ also make effective masses for electrons and holes unequal,[35] in agreement with the findings from the Raman scattering.[14]

In our experiments, we have measured the optical reflection $R(\Omega, V_g)$ and transmission $T(\Omega, V_g)$ as a function of the frequency Ω and the gate voltage V_g. From R and T we extracted the real and imaginary part of the conductivity using a commercial software package. Some of these experimental results were reported previously.[28]

In this paper we present more extensive experimental data and we also compute the same three quantities — σ, R, and T — theoretically. The calculation requires accounting for the interplay of three physical phenomena: (a) electrostatic charging of the layers (b) their dynamical conductivity, and (c) the optical properties of the environment (sample, substrate, and the gate). Each of these ingredients has been studied in the past.[21,22,31–33,36] However, in this work we carry out a self-contained calculation, which enables us to directly compare our theoretical results with the measurements.

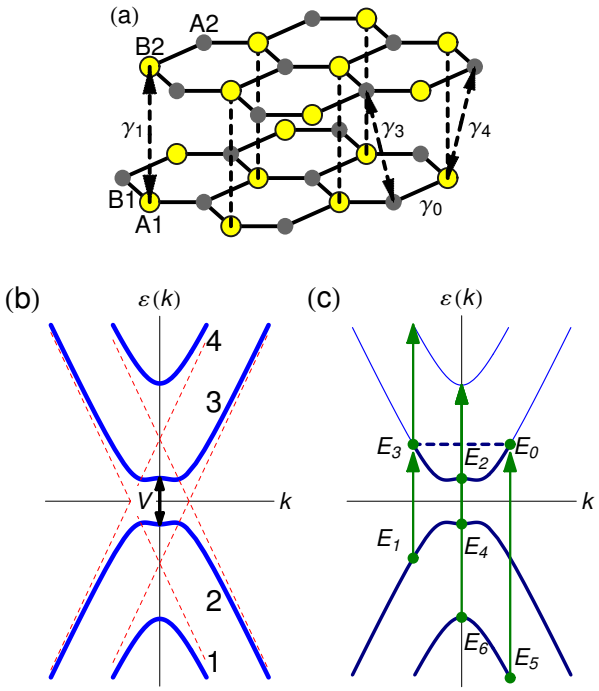

FIG. 1: (Color online) (a) Crystal structure of the graphene bilayer with the relevant SWMc hopping parameters shown (b) Band structure of a biased bilayer (lines), which can be considered as hybridization of two shifted Dirac cones (dots). Numbers on the right label the four bands. (c) Examples of the allowed optical transitions for the chemical potential indicated by the dashed line. Occupied states are shown by the thicker lines. The dots and the arrows mark the initial and the final states, respectively, of the transitions that produce features at frequencies E_j, $j = 1, 2, \ldots, 6$ in Fig. 2(a) below. E_0 is the intraband transition (Drude peak).

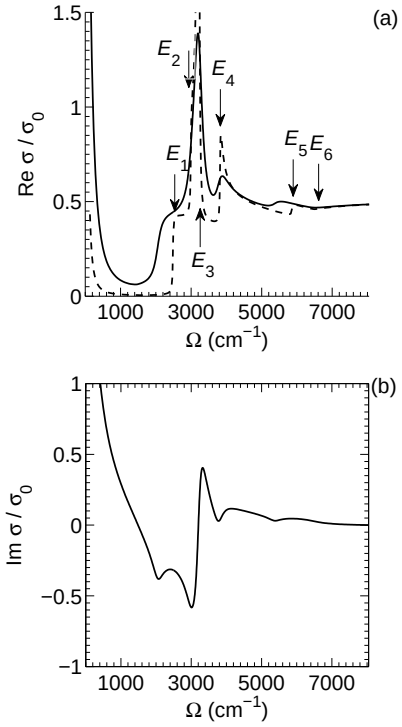

FIG. 2: (a) Real and (b) imaginary part of conductivity in units of $\sigma_0 = e^2/\hbar$ for the gate voltage $V_g = -100\,\mathrm{V}$ and $v_4 = 0.1\gamma_1$. The solid curves are for broadening $\Gamma = 0.02\gamma_1$. The dashed curve is for $\Gamma = 0.002\gamma_1$.

The remainder of the paper is organized as follows. In Sec. II we summarize our results. Theoretical derivation is outlined in Sec. III. Section IV contains comparison of the theory and experiment, discussion, and conclusions. Some calculational details are relegated to the Appendix.

II. RESULTS

To measure the optical response of the bilayer we employed synchrotron infrared radiation, as described previously.[28,37] Understandably, the two-atom thick sample has a rather small optical signal. The quantity which can be extracted most reliably from the current experiments is the relative transmission $T(\Omega, \delta V)/T(\Omega, V_{\mathrm{CN}})$ and reflection $R(\Omega, \delta V)/R(\Omega, V_{\mathrm{CN}})$. All measurements wer done at the temperature of 45 K. The data for the largest $|\delta V|$ are depicted in Fig. 3. The main feature in the relative transmission spectra is a small but clearly visible dip around $\Omega = 3200\,\mathrm{cm}^{-1}$. Away from the dip, the relative transmission is slightly higher than unity. The relative reflection spectra are characterized by a dip-peak structure. Transmission and reflection spectra are asymmetic between positive and negative δV, which correspond, respectively, to doping of electrons and holes in bilayer graphene.

From the transmission and reflectance data, we extracted the optical conductivity.[28,37,38] The dominant feature in the conductivity spectra is a strong peak at $\Omega \approx 3200\,\mathrm{cm}^{-1}$, see Fig. 4(b). Below that frequency, we observed a broadened threshold feature, which shifts systematically with δV. The most intriguing observation is again a significant asymmetry in the optical conductivity. For instance, the frequencies of the main peak in $\mathrm{Re}\,\sigma(\Omega)$ and its voltage dependence are noticeably different on the electron and hole sides, see Fig. 4(b).

On the theory side, we calculated σ, T, and R, using the SWMc constants and Γ as adjustable parameters. Results for the conductivity are shown in Fig. 4(a). For the reflection and transmission, see Fig. 3. The parameters were adjusted to reproduce the frequency positions and widths of the main features of the experimental data, as discussed below. Their vertical scale is also in a reasonable agreement with the calculations.

Both in our experiment and in calculations the carrier concentrations are always smaller than the characteristic value n_0 given by

$$n_0 = \frac{\gamma_1^2}{\hbar^2 v^2} = 3.7 \times 10^{13}\,\mathrm{cm}^{-2}\,. \qquad (1)$$

Here and below we assume that $\gamma_0 = 3.0\,\mathrm{eV}$, which corresponds to $v = (3/2)\gamma_0 a/\hbar = 1.0 \times 10^8\,\mathrm{cm}/s$. (Based on other results in the literature, this value should be accurate to about 10%.) At concentrations $|n| < n_0$ the high energy bands 1 and 4 have no free carriers and $\mathrm{Re}\,\sigma(\Omega)$ has a pronounced peak at $\Omega \approx 3200\,\mathrm{cm}^{-1}$. As explained above, this feature corresponds to transition between band pairs that are nearly parallel: bands 3 and 4 for $\mu > 0$ or bands 1 and 2 for $\mu < 0$, see Fig. 1.

The evolution of the infrared response with V_g can be understood as follows. As the gate voltage deviates further away from V_{CN}, the electron concentration

$$n = C_b \delta V/e \qquad (2)$$

and the chemical potential μ increase by the absolute value. Here C_b is the capacitance between the bilayer and the gate. As a result of an increased $|n|$, the peak become more pronounced. Simultaneously, near the higher frequency side of the peak a depletion of conductivity develops. One can say that the optical weight is increasingly transfered from the high frequencies to the γ_1 peak. Larger conductivity is directly associated with decreased optical transmission. Therefore one observes an increasing dip in the transmission near γ_1 and a higher transmission at higher Ω, see Fig. 3. Similar features appear in the reflection but they are more difficult to interpret as they are also affected by $\mathrm{Im}\,\sigma(\Omega)$.

Very important for our analysis are the aforementioned small shifts in the position of the γ_1 peak as a function of δV. Within the SWMc model, their origin is as follows. In the absence of broadening, the peak arises from the absorption in the range of frequencies, $E_2 < \hbar\Omega < E_3$, see Figs. 1 and 2. Since the optical weight at E_3 is higher, the

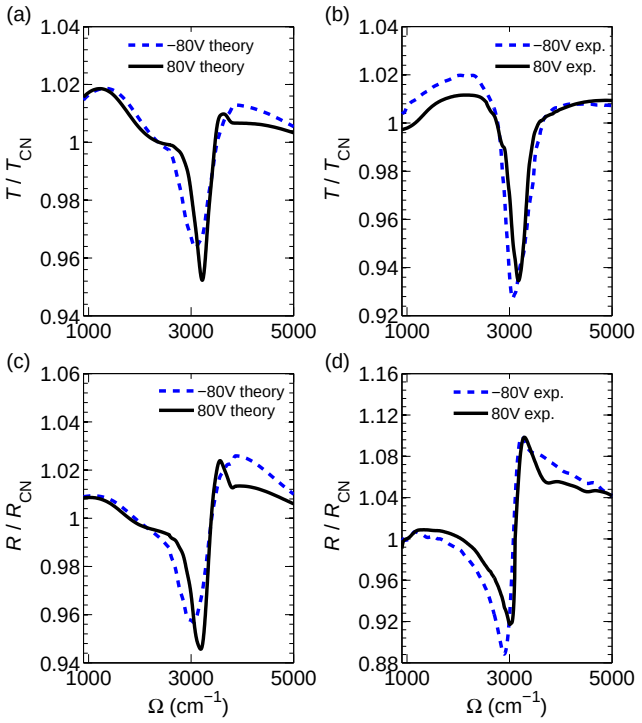

FIG. 3: (Color online) Relative transmission: (a) theory (b) experiment. Relative reflection: (c) theory (d) experiment. The solid line is for electrons, $\delta V \approx +80\,\mathrm{V}$. The dashed line is for holes, $\delta V \approx -80\,\mathrm{V}$. The experimental uncertainties are ~ 0.002 at Ω near $3000\,\mathrm{cm}^{-1}$ and ~ 0.005 at high frequency.

conductivity peak occurs at energy E_3. However, if the broadening is large enough, the optical weight becomes distributed more uniformly, and the peak position moves to the midpoint of E_2 and E_3, see Fig. 5. Energies E_2 and E_3 themselves vary with the gate voltage (or n). For positive δV (positive n), $E_2 \equiv E_2^+$ is the energy difference between the bands 3 and 4 at $k = 0$. The energy $E_3 \equiv E_3^+$ is the corresponding difference at $k = k_F$, where

$$k_F = \mathrm{sign}\,(n)\sqrt{\pi|n|} \qquad (3)$$

is the Fermi momentum. For $\delta V < 0$ we denote E_2 and E_3 by, respectively, E_2^- and E_3^- and they are computed using the bands 1 and 2 instead of 3 and 4.

From the band structure,[21,22] we can find the following approximate expressions valid for $n \ll n_0$:

$$E_2^{\pm} \simeq \gamma_1 - \frac{V}{2} \pm \Delta\,, \qquad (4)$$

$$E_3^{\pm} \simeq \gamma_1\sqrt{1 + \frac{2\pi|n|}{n_0}} - \sqrt{\frac{V^2}{4} + \left(\frac{\pi\gamma_1 n}{n_0}\right)^2} \pm \Delta \mp 2\left(2v_4\gamma_1 + \Delta\right)\frac{\pi|n|}{n_0}\,. \qquad (5)$$

Here $V = V(n)$ as well as the chemical potential $\mu = \mu(n)$ are determined self-consistently by the electrostatics of the system,[36] see Sec. III These equations indicate

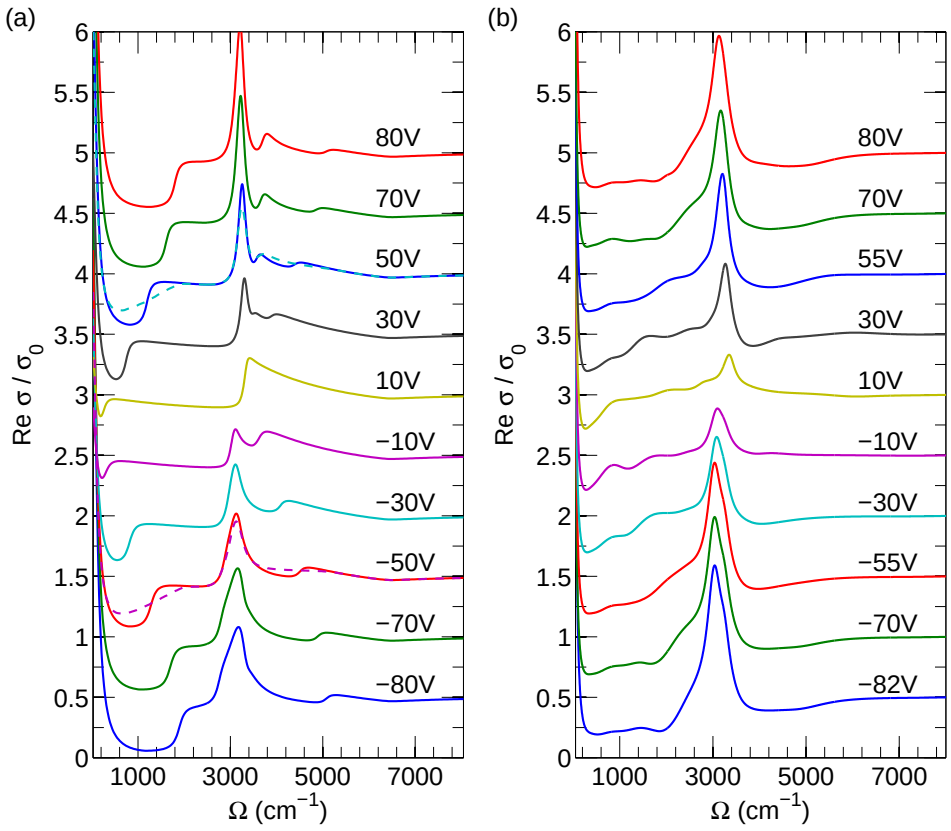

FIG. 4: (Color online) Theoretical (a) and experimental (b) results for the conductivity Re $\sigma(\Omega)$. The deviation $\delta V = V_g - V_{\rm CN}$ of the gate voltage from the charge neutrality point is indicated next to each curve. For clarity, the curves are offset vertically by $0.5\sigma_0$ from one another. Here $\sigma_0 = 4e^2/\hbar$. The dashed curves superimposed on the $\delta V = +50$ V (-50 V) traces are the arithmetic means of all the positive (negative) δV curves. Their significance is discussed in the main text.

that the parameters primarily responsible for electron-hole asymmetry are γ_4 and Δ.

Physically, Δ is the difference of the on-site electron energies of the A and the B sites[6,7] [the stacked and unstacked sublattices, respectively, see Fig. 1(a)]. It has two effects: first, it lifts the $k = 0$ energy for bands 1 and 4; second, it adds a k dependent perturbation to the two band dispersion. Parameter $v_4 = v\gamma_4/\gamma_0$ of dimension of velocity characterizes hopping between a stacked atom and its the three unstacked neighbors of its stacking partner. It also introduces difference between the valence and conduction bands. To the leading order in k, this hopping shifts the two middle bands (2 and 3) upward by a term proportional to v_4k^2 and shifts the two outer bands (1 and 4) downward by the same amount. These effects of Δ and v_4 are illustrated in Fig. 6.

Additional electron-hole asymmetry can in principle come from extrinsic sources, e.g., charged impurities that can be present on or between the layers. Besides creating a finite $V_{\rm CN}$, these charges also move $V = 0$ point away from the charge neutrality point $n = 0$. To the first approximation,[36] this introduces an offset of the interlayer bias: $V(n) \to V(n) + V_0$. However, our calculations suggest that for reasonable V_0 this effect has a smaller influence on the electron-hole asymmetry of the optical response than Δ and γ_4.

Based on the above discussion, we can predict qualitatively how the position of the main conductivity peak should vary as a function of δV. For example, on the electron side, and for $v_4 > 0$, the peak should move to lower frequencies as δV increases. Alternatively, this can be seen from Fig. 6: the top two bands move closer to each other as $k = k_F$ increases.

For the quantitative analysis, we use a full numerical calculation of σ and T, which is discussed in Sec. III below. It demonstrates that for the case of small Γ the energy E_3 is indeed in an excellent agreement with the computed peak positions. However, the broadening observed in experiments[28–30] is appreciable. For the corresponding Γ other nearby transitions, E_1 and E_4, start to influence the main peak. As a result, although the formula $\Omega_0 = (E_2 + E_3)/2$ is in general a good indicator of the peak position, it fails to capture the dependence of Ω_0 on V_g in all its detail. Hence, for comparison with experiment we use our numerical results rather than Eqs. (4) and (5).

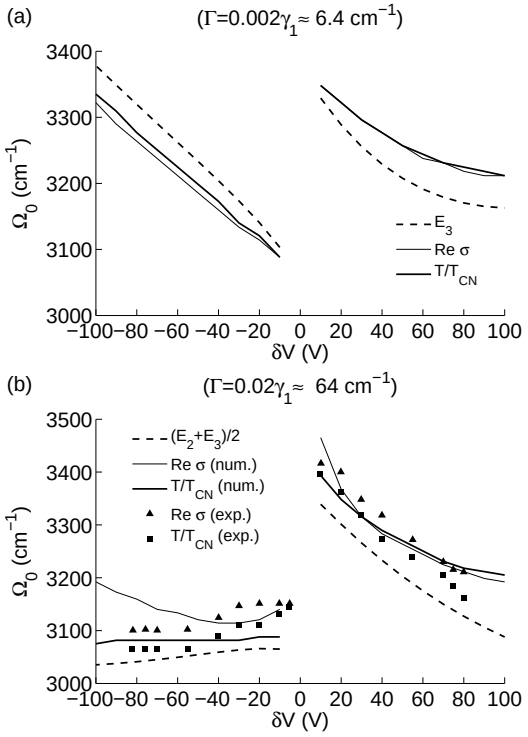

FIG. 5: Position of the γ_1 feature versus gate voltage for $\gamma_1 = 0.40\,\text{eV}$, $\gamma_4 = 0.15\,\text{eV}$, $\Delta = 0.02\,\text{eV}$ and the two values of broadening (a) $\Gamma = 0.02\gamma_1$ and (b) $\Gamma = 0.002\gamma_1$. The thin solid lines are our numerical results from the conductivity and the thick ones are from the relative transmission. The dashed lines show E_3 and $(E_2 + E_3)/2$ in the cases (a) and (b), respectively. The symbols are our experimental results.

Fitting these numerical results to the data, see Fig. 5, we have obtain estimates of γ_1, γ_4, and Δ listed in Table I. This fitting procedure proved to be very straightforward. For example, Δ is determined mostly by the splitting of the peak positions on the electron and the holes sides of the charge neutrality point. Parameter γ_1 is essentially the average of the two. Finally, γ_4 controls the slope of the $\Omega_0(V_g)$ curves away from V_{CN}. Therefore, all these parameters can be uniquely determined.

In Table I we also list SWMc values suggested in prior literature. They mainly agree with ours for the principal SWMc parameters γ_0 and γ_1 but show some deviations for the more subtle quantities γ_4 and Δ we have been discussing here. Possible reasons for these differences are discussed in Sec. IV.

III. DERIVATION

A. Band structure

The bilayer is two monolayers stacked together, see Fig. 1(a). In the bulk graphite the preferential stacking is the AB (Bernal) one, such that only one sublattice of each layer is bonded to each other. In order to achieve agreement with experiments,[28] we have to assume that in the bilayer the stacking is the same. We use the basis $\{\Psi_{A1}, \Psi_{B1}, \Psi_{B2}, \Psi_{A2}\}$, where the letter stands for the sublattice label and the number represents the layer index. In this basis the SWMc tight-binding Hamiltonian for the bilayer becomes[22]

$$\mathcal{H}_2 = \begin{pmatrix} -\frac{V}{2}+\Delta & \phi & \gamma_1 & -v_4\phi^* \\ \phi^* & -\frac{V}{2} & -v_4\phi^* & v_3\phi \\ \gamma_1 & -v_4\phi & \frac{V}{2}+\Delta & \phi^* \\ -v_4\phi & v_3\phi^* & \phi & \frac{V}{2} \end{pmatrix}, \qquad (6)$$

where $\phi = k_x + ik_y$ and (k_x, k_y) is the in-plane momentum. In the following we set $v_3 \equiv \gamma_3/\gamma_0$ to zero for reasons explained in Sec. IV.

Given V, it is easy to obtain the four band energies $\varepsilon_\alpha(k)$ and the corresponding eigenstates $|\alpha, \mathbf{k}\rangle$ by numerical diagonalization of the above Hamiltonian. However, as mentioned in Sec. II, V should be determined self-consistently as a function of V_g, or equivalently, the total carrier concentration n. The algorithm for doing so is given next.

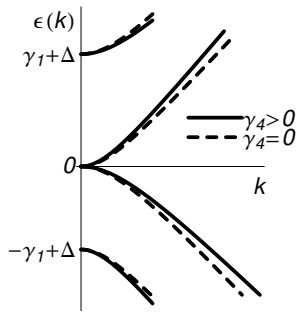

FIG. 6: The effect of γ_4 and Δ on the band structure. Parameter Δ raises the bands 1 and 4. The interlayer neighbor hopping term γ_4 gives a contribution quadratic in k opposite in sign for the conduction and the valence bands. The solid (dashed) lines are the bands with positive (zero) value of γ_4.

B. Electrostatics

As discussed in the literature,[22,36] the electric field of the gate has two major effects on the bilayer graphene. First, it modifies the bands by introducing a potential difference between the layers and as a consequence opens up the energy gap. Second, it induces charge carriers. Electric field of the charged impurities can play a similar role: it creates a layer asymmetry V_0 and opens a

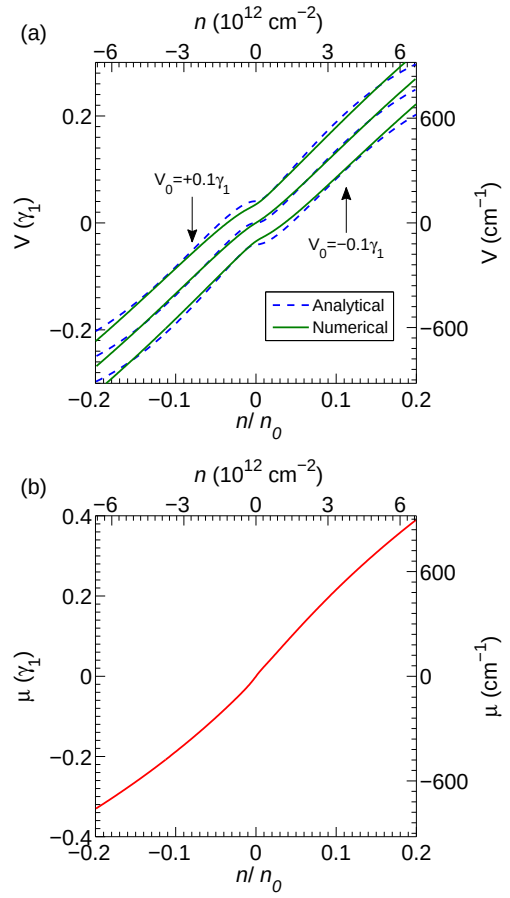

FIG. 7: (a) Interlayer bias V and (b) chemical potential μ as function of total density n. Three sets of curves in (a) correspond to three values of V_0, from top to bottom: $0.1\gamma_1, 0, -0.1\gamma_1$. The curve in (b) correspond to $V_0 = -0.1\gamma_1$. The curve labelled "Analytical" is computed from Eq. (12).

gap at the charge neutral point much like an external gate. But the more important effect of the impurities is presumably the broadening of the electron energy states, which we describe by a phenomenological constant Γ. For example, if the impurities are distributed symmetrically between the two layers, then V_0 is zero but Γ is still finite. For simplicity, we assume Γ to be independent of energy, momentum, or a band index.

To compute $V(n)$ and $\mu(n)$ we set up a system of equations similar to those in Refs. 36 and 21. These equations capture the dominant Hartree term of the interaction but neglect exchange and correlation energies.[18] The first equation is [cf. Eq. (2)]

$$n = n_t + n_b = C_b \delta V/e\,, \tag{7}$$

where n_t and n_b are the carrier concentrations of the top and bottom layers, $and C_b$ is the capacitance to the gate. Second, the electrostatic potential difference between the two layers V is given by

$$V = \frac{4\pi e^2}{\kappa}(n_t - n_b)c_0\,, \tag{8}$$

where κ is the dielectric constant and c_0 is the distance between the layers. Next, the Hamiltonian and therefore wavefunction and the layer density n_t and n_b depend on V. Therefore the quantities V, n_t, and n_b must be solved for self-consistently. If the broadening Γ is neglected, this can be done analytically in the limit $V, \mu \ll \gamma_1$, which gives $V \simeq \mathcal{V}(n, V_0)$, where[21,36]

$$\mathcal{V}(n, V_0) = \frac{X\gamma_1 + V_0}{\Lambda^{-1} + |X| - \frac{1}{2}\ln|X|}\,, \quad X = \frac{\pi n}{n_0}\,, \tag{9}$$

n_0 is defined by Eq. (1), and $\Lambda \equiv e^2 c_0 n_0/(\pi\kappa\gamma_1)$ is the dimensionless strength of the interlayer screening. Using the typical parameter values, one estimates[36] $\Lambda \sim 1$, and so the interlayer screening is significant.[18,36]

For experimentally relevant broadening $\Gamma \sim 0.02\gamma_1$, the approximation leading to Eq. (9) is no longer accurate. Therefore, we computed the dependence of n_t and n_b on V numerically as follows. We first define the retarded Green's function $\mathbf{G}^R$ by the analytic continuation $\mathbf{G}^R(\varepsilon) = \mathbf{G}(\varepsilon \to \varepsilon + i\Gamma)$ of the following expression

$$\mathbf{G} = \sum_{\alpha=1}^{4} \frac{1}{\varepsilon - \varepsilon_\alpha(k)} |\alpha, \mathbf{k}\rangle \langle \alpha, \mathbf{k}|\,. \tag{10}$$

Then we compute n_t from

$$n_t = -\int \frac{d^2k}{(2\pi)^2} \int_{-\infty}^{\mu} \frac{d\varepsilon}{\pi} \mathrm{Im}[G^R_{11}(\mathbf{k}, \varepsilon) + G^R_{22}(\mathbf{k}, \varepsilon)]\,, \tag{11}$$

using numerical quadrature. Similarly, the formula for n_b is obtained by replacing $G_{11} + G_{22}$ with $G_{33} + G_{44}$.

The system of nonlinear equations (7), (8), and (11) is solved by an iterative procedure. For a given chemical potential μ we start from some initial guess on V. Then we diagonalize the Hamiltonian and compute $\mathbf{G}^R$, n_t, and n_b. Substituting them into Eq. (8), we get the value of V for the next iteration. (Actually, we use not this value directly but a linear combination of the new and old V.) The iterations terminate when the values of V changes by less than a desired relative accuracy (typically, 10^{-5}). The results of these calculations are in a good agreement with Eq. (9) for $\Gamma = 0$, and so are not shown. On the other hand, the results for $\Gamma = 0.02\gamma_1$, which are plotted in Fig. 7, appreciably deviate from Eq. (9). The agreement greatly improves (see Fig. 7) if instead of Eq. (9) we use, on heuristic grounds, the following formula:

$$V(n) = \mathcal{V}(n_*, V_0) - \mathcal{V}(n_\Gamma, 0)\,, \tag{12}$$

$$n_* = \mathrm{sign}(n)\sqrt{n^2 + n_\Gamma^2}\,, \quad n_\Gamma = \mathrm{sign}(n)\frac{2\Gamma n_0}{\pi\gamma_1}\,. \tag{13}$$

C. Dynamical Conductivity

The above procedure enables us to compute V and n for a given chemical potential μ. With the former determining the Hamiltonian and therefore its eigenstates, and

the latter determining their occupancy, we can now compute the dynamical conductivity by the Kubo formula[39]

$$\sigma_{xx}(\Omega) = i\,\frac{\Pi^R_{xx}(\Omega) - \Pi^R_{xx}(0)}{\Omega + i0}\,, \tag{14}$$

where the polarization operator $\Pi^R_{xx}(\Omega)$ is given by

$$\Pi^R_{xx}(\Omega) = ig\frac{e^2}{\hbar^2}\int\frac{d^2k}{(2\pi)^2}\int\limits_{-\infty}^{\mu}\frac{d\varepsilon}{2\pi}\mathrm{Tr}\left\{\mathbf{v}_x\left[\mathbf{G}^R(\mathbf{k},\varepsilon) - \mathbf{G}^A(\mathbf{k},\varepsilon)\right]\mathbf{v}_x\left[\mathbf{G}^R(\mathbf{k},\varepsilon+\Omega) + \mathbf{G}^A(\mathbf{k},\varepsilon-\Omega)\right]\right\}. \tag{15}$$

In this equation $g = 4$ is the spin-valley degeneracy of graphene, $\mathbf{v}_x = \partial\mathbf{H}/\partial k_x = \sigma_x \otimes \mathbf{I}$ is the velocity operator, σ_x is the Pauli matrix, and $\mathbf{G}^{R,A}$ at the retarded and the advanced Green's functions. Assuming again that the broadening is momentum and energy independent, these functions are obtained by the analytic continuation of $\mathbf{G}$ in Eq. (10): $\mathbf{G}^{R,A}(\varepsilon) = \mathbf{G}(\varepsilon \to \varepsilon \pm i\Gamma)$. After some algebra, we find

$$\Pi^R_{xx}(\Omega) = ig\left(\frac{e}{\hbar}\right)^2\int\frac{d^2k}{(2\pi)^2}\sum_{\alpha,\beta}|M_{\alpha\beta}(\mathbf{k})|^2\sum_{\xi,\zeta=\pm1}\xi K\left[\varepsilon_\beta(k) - i\Gamma\xi,\ \varepsilon_\alpha(k) - (i\Gamma + \Omega)\,\zeta\right], \tag{16}$$

where $M_{\alpha\beta}(\mathbf{k}) = \langle\alpha,\mathbf{k}\,|\sigma_x\otimes\mathbf{I}|\,\beta,\mathbf{k}\rangle$ is the interband transition matrix element, and function K is given by

$$K(z_1,z_2) = \frac{\ln(\mu - z_1) - \ln(\mu - z_2)}{2\pi(z_1 - z_2)} \tag{17}$$

with the branch cut for $\ln z$ taken to be the negative real axis.

For zero V and Γ the conductivity can be computed in the closed form, see Appendix B. For other cases, we evaluated it numerically. The result is shown in Fig. 2. The real part of the conductivity is plotted for large and small Γ in Fig. 2(a). In the latter of the smaller broadening, one can easily identify all six transition energies, in agreement with previous calculations.[21,22,31,33] As explained above, the interband transition at $\Omega \approx 3200\,\mathrm{cm}^{-1}$ shows up as a pronounced peak because E_2 and E_3 are close in energy and the optical density of state is high at frequencies $E_2 < \Omega < E_3$. The other tall feature at $\Omega = 0$ is the intraband Drude peak.

IV. DISCUSSION

In this paper we presented a joint experimental and theoretical study of the infrared response of a bilayer graphene. Our results demonstrate a complex interplay among various interband transitions and their disorder-induced broadening. Nevertheless, by means of a careful analysis, we have been able to explain the major observed features within the conventional SWMc model. The corresponding SWMc parameters are given in Table I, together with their estimated uncertainties. In particular, our γ_1 should have a very high accuracy: at least $100\,\mathrm{cm}^{-1}$, i.e., 3%, or better.

Let us now compare our SWMc parameters with those found in previous work on bilayers and bulk graphite. For the bilayer case there is at present only one other experimental determination[14] of γ_j's. From Table I we see that the difference between our and their values are primarily in γ_1 and γ_4. Actually, our SWMc parameters can describe the Raman data equally well[40] as the parameters given in Ref. 14. Our parameter values have smaller estimated errors and should be considered more accurate.

For the bulk graphite, we see a good agreement with the set of parameter obtained by Dillon *et al.*[9] On the other hand, it differs from the set recommended by the MIT group,[8] especially for γ_4 and Δ. Parameter Δ even has the opposite sign. Recent experimental[20] and theoretical[13] studies have not yet come to a consensus on this issue. We feel that further work is needed to settle this discrepancy. Meanwhile, we can argue Δ in the bilayer and in bulk graphite may not be the same. Recall that the physical meaning of Δ is the difference in the onsite energies of the A and B sublattices[7] due to the interlayer coupling. Its physical mechanism is presumably the short-range (exponentially decaying with distance) exchange and correlation interactions between the electron states of the stacking partners. Indeed, it has been pointed out repeatedly[41,42] that neither Coulomb nor even the van der Waals interaction have short enough range to discriminate between the two sublattices, given the relatively large interlayer distance of the graphite.

For this reason, we think that only the interactions among the nearest and the next-nearest neighbor layers are important for Δ. (This is also in the spirit of the SWMc model.) Actually, in the Bernal (or AB) graphite the next-nearest-layer interactions cannot contribute to Δ simply by symmetry. This leaves us with the nearest-

neighbor terms. Since Δ is numerically small, we can argue that it can be studied by the perturbation theory. In the bilayer each A atom has a single stacking partner but in the Bernal graphite it has two of them, and so naively we expect $\Delta_{\text{graphite, AB}} \approx 2\Delta_{\text{bilayer}}$. In real graphite samples, which usually contain other stacking orders (rhombohedral and turbostratic), the ratio $\Delta_{\text{graphite}}/\Delta_{\text{bilayer}}$ can be less than 2. This crude argument assumes of course that the interlayer distance in the bilayer and in the graphite are exactly the same, which may not be the case. Measurements of trilayers and tetralayers may shed further light on the question of the apparent difference of the SWMc parameters in few-layer and bulk graphite systems.

Returning to the possible discrepancy in γ_4, we note that our estimate of γ_4 can be defended on the grounds that it is comparable to the accepted value of γ_3. These two parameters describe hopping between pairs of atoms at equal distances in the lattice, see Fig. 1(a), and theoretically are not expected to be vastly different from each other. Large difference of γ_4 between the bilayer and the bulk graphite is not expected either. Indeed, even when they disagree about the order of magnitude (or sign) of Δ, all electronic structure calculations to date find that $\gamma_4 \sim \gamma_3$ and are of the same order of magnitude in the two systems, see Table I.

Parameter γ_3 itself cannot be reliably extracted from the experimental data[28] we analyzed here. At the relevant carrier concentrations the main effect of γ_3 is to produce a weak trigonal warping of the band dispersion.[8] This warping averages out over the Fermi surface, and does not affect the position of the γ_1 conductivity peak. It does contribute to the broadening Γ of the peak; however, it is difficult to separate this effect from the broadening due to disorder.

Finally, regarding the latter, the dc mobility that we find from our numerically computed $\sigma(0)$ using $\Gamma = 0.02\gamma_1 \approx 8\,\text{meV}$ is $\mu \approx 3900\,\text{cm}^2\,/\,\text{Vs}$. This is close to the transport mobility typical for bilayer graphene, supporting our interpretation that Γ arises mainly due to disorder.

One feature of the experimental data that is not accounted for by our model is an unexpectedly large amount of the optical weight in a range of frequencies below the γ_1 peak. It is present between the Drude peak and 2μ, i.e., twice the chemical potential. For the chosen Γ, our calculation predicts $\text{Re}\,\sigma(\Omega) \sim 0.02e^2/\hbar$ at such Ω, see Fig. 3, whereas the measured value is a few times larger.[28] This extra weight is present also in the monolayer graphene, in the same range of frequencies.[37] A related issue is a very gradual rise of $\text{Re}\,\sigma(\Omega)$ around the point $\Omega = 2\mu$ compared to a sharp threshold expected theoretically.

We can tentatively attribute both the broadening of the $\Omega = 2\mu$ threshold and the extra weight at $\Omega < 2\mu$ to significant long-range density inhomogeneities in the sample. They can be caused by charge impurities and remnants of the photoresist used in the sample processing. The presence of such inhomogeneities would modulate the local chemical potential, and so in the infrared response one would see a certain average of the $\sigma\,(\Omega)$ taken at different δV. We illustrate this argument by calculating the arithmetic mean of $\sigma\,(\Omega)$'s for positive (negative) δV and superimposing the results (shown by the dashed lines) on the $\sigma\,(\Omega)$ traces for $\delta V = +50\,\text{V}$ $(-50\,\text{V})$ in Fig. 4(a). Such averaged conductivities indeed resemble the experimental data [Fig. 4(b)] more faithfully. A more quantitative analysis of this scenario warrants further work.

APPENDIX A: REFLECTION AND TRANSMISSION

To compute the transmission coefficient T and the reflection coefficient R we follow the standard procedure.[43] In general, the result depends on the angle of incidence and on the polarization of light. Abergel and Fal'ko[44] derived the formulas for R and T for the S-polarization where the electric field is perpendicular to the plane of incidence (and parallel to the sample surface). We reproduce them here with a slight change in notation:

$$\begin{aligned} R &= \left| -\frac{C\,n_1\cos\theta_1 - D\,[\cos\theta_0 - 4\pi\sigma]}{C\,n_1\cos\theta_1 + D\,[\cos\theta_0 + 4\pi\sigma]} \right|^2 , \\ T &= \left| -\frac{2\cos\theta_0\; n_1\cos\theta_1\; n_2\cos\theta_2}{C\,n_1\cos\theta_1 + D\,[\cos\theta_0 + 4\pi\sigma]} \right|^2 , \end{aligned} \tag{A1}$$

where A, B, C, and D are given by

$$\begin{aligned} A &= \cos\theta_2 \sin\delta_2 + i n_2 \cos\theta_0 \cos\delta_2 \,, \\ B &= i\cos\theta_2 \cos\delta_2 + n_2 \cos\theta_0 \sin\delta_2 \,, \\ C &= A\,n_1 \cos\theta_2 \sin\delta_1 + iB\,n_2 \cos\theta_1 \cos\delta_1 \,, \\ D &= iA\,n_1 \cos\theta_2 \cos\delta_1 + B\,n_2 \cos\theta_1 \sin\delta_1 \,. \end{aligned} \tag{A2}$$

In Eqs. (A1) and (A2), the index $j = 0, 1, 2$ represents vacuum, SiO_2, and Si layers respectively, n_j are the index of refraction of each layer, and θ_j are the angles the light ray makes with the surface normal in each layer. They satisfy Snell's law $n_j \sin\theta_j = \text{const}$. Finally, $\delta_j = kL_j/n_j$ is the phase the light picks up as it makes one pass across the layer of thickness L_j.

For the other, P-polarization, where the electric field is not exactly parallel to the surface of the sample, we find a different expression:

$$\begin{aligned} R &= \left| \frac{C\,n_1\cos\theta_0 - D\,\cos\theta_1\,(1 - 4\pi\sigma\cos\theta_0)}{C\,n_1\cos\theta_0 + D\,\cos\theta_1\,[1 + 4\pi\sigma\cos\theta_0]} \right|^2 , \\ T &= \left| \frac{-2\cos\theta_0\,n_1\cos\theta_1\,n_2\cos\theta_2}{C\,n_1\cos\theta_0 + D\,\cos\theta_1\,[1 + 4\pi\sigma\cos\theta_0]} \right|^2 . \end{aligned} \tag{A3}$$

For this polarization the conductivity enters R and T multiplied by a cosine of the angle of incidence, i.e., its

effect is reduced. In our experiments, we typically have $\theta_0 \sim 30^\circ$, and so this reduction is quite small. It was not included in the analysis.

APPENDIX B: CONDUCTIVITY OF AN UNBIASED BILAYER AT VANISHING BROADENING

The conductivity for the case $\Gamma = V = 0$ was computed previously in Refs. 31 and 44. In our attempt to reproduce their formula we discovered that it contains a typographical sign error.[45] For future reference, we give the corrected expression below.

In the limit of zero broadening, $\Gamma \to 0$, Eqs. (14)–(17) reduce to the following expression for the conductivity:

$$\sigma(\Omega) = \frac{ge^2v^2}{2i\pi\hbar} P\int_0^\infty \frac{d\omega}{\omega} \frac{\Omega |M_{\alpha\beta}|^2}{\omega^2 - (\Omega + i0)^2} \sum_j k_j(\omega) k_j'(\omega)\,, \tag{B1}$$

where P means principal value and the integration variable $\omega = |\varepsilon_\alpha - \varepsilon_\beta|$ is the energy difference between two states. The sum in Eq. (B1) is over all values of momentum $k_j(\omega)$ of which two states differing in energy ω exist. For $V = 0$ where the the matrix elements $M_{\alpha\beta}$ take a simple form, the integration over ω in Eq. (B1) can be done analytically. The result can be written as a sum of three terms:

$$\frac{\sigma(\Omega)}{\sigma_0} = \tilde\sigma_0(\Omega) + \tilde\sigma_{\gamma_1}(\Omega) + \tilde\sigma_{2\gamma_1}(\Omega)\,, \tag{B2}$$

where $\sigma_0 = e^2/\hbar$ is the unit of conductivity, $\tilde\sigma_0$ is contribution from transitions between bands 2 and 3 that turn on at $\Omega = 0$, $\tilde\sigma_{\gamma_1}$ is contribution from transitions between bands 1 and 3 and bands 2 and 4 that turn on at $\Omega = \gamma_1$, $\tilde\sigma_{2\gamma_1}$ is contribution from transition between bands 1 and 4 that turn on at $\Omega = 2\gamma_1$. They are given by

$$\tilde\sigma_0 = \frac{g}{8}\left[\frac{1}{2}\frac{\Omega + 2\gamma_1}{\Omega + \gamma_1} - \frac{i}{\pi}\frac{\Omega\gamma_1}{\gamma_1^2 - \Omega^2}\ln\left|\frac{\Omega}{\gamma_1}\right|\right]\,, \tag{B3a}$$

$$\tilde\sigma_{\gamma_1} = \frac{g}{8}\left[\frac{\gamma_1^2}{\Omega^2}\Theta(\Omega - \gamma_1) + \frac{i}{\pi}\left(\frac{2\gamma_1}{\Omega} - \frac{\gamma_1^2}{\Omega^2}\ln\left|\frac{\gamma_1 + \Omega}{\gamma_1 - \Omega}\right|\right)\right]\,, \tag{B3b}$$

$$\tilde\sigma_{2\gamma_1} = \frac{g}{8}\left[\frac{1}{2}\frac{\Omega - 2\gamma_1}{\Omega - \gamma_1}\Theta(\Omega - 2\gamma_1) - \frac{i}{\pi}\left(\frac{1}{2}\frac{\Omega^2 - 2\gamma_1^2}{\Omega^2 - \gamma_1^2} \times \ln\left|\frac{2\gamma_1 + \Omega}{2\gamma_1 - \Omega}\right| + \frac{1}{2}\frac{\Omega\gamma_1}{\Omega^2 - \gamma_1^2}\ln\left|\frac{4\gamma_1^2 - \Omega^2}{\gamma_1^2}\right|\right)\right]\,, \tag{B3c}$$

where, for ease of notation, Ω stands for $\hbar\Omega$ and $g = 4$.

[1] K. S. Novoselov, A. K. Geim, S. V. Morozov, D. Jiang, Y. Zhang, S. V. Dubonos, I. V. Grigorieva, and A. A. Firsov, Sci. **306**, 666 (2004).

[2] Y. Zhang, J. P. Small, M. E. S. Amori, and P. Kim, Phys. Rev. Lett. **94**, 176803 (2005).

[3] For a review, see A. H. Castro Neto, F. Guinea, N. M. R. Peres, K. S. Novoselov, and A. K. Geim, arXiv:0709:1164; Rev. Mod. Phys., in press.

[4] P. R. Wallace, Phys. Rev. **71**, 622 (1947).

[5] J. C. Slonczewski and P. R. Weiss, Phys. Rev. **109**, 272 (1958).

[6] J. W. McClure, Phys. Rev. **108**, 612 (1957).

[7] J. L. Carter and J. A. Krumhansl, J. Phys. Chem. **21**, 2238 (1953).

[8] For a review, see M. S. Dresselhaus and G. Dresselhaus, Adv. Phys. **30**, 139 (1981). Reprinted as Adv. Phys. **51**, 1 (2002).

[9] R. O. Dillon, I. L. Spain, and J. W. McClure, J. Phys. Chem. Solids **38**, 635 (1977).

[10] For example, in the often cited book of Brandt *et al.*[46] the sign of Δ is shown as positive whereas the original source[8,47] is very clear on it being negative. This incorrect sign has propagated into Nilsson *et al.*[22] and Malard *et al.*[14] Nilsson *et al.*[22] also misquoted both γ_5 and Δ when citing another review.[48] To make it even more confusing, this review, which is otherwise fairly up-to-date, chose nevertheless to cite an early[49] (later revised[8]) parameter determination from the MIT group.

[11] R. C. Tatar and S. Rabii, Phys. Rev. B **25**, 4126 (1982).

[12] J.-C. Charlier, X. Gonze, and J.-P. Michenaud, Phys. Rev. B **43**, 4579 (1991).

[13] A. Grüneis, C. Attaccalite, T. Pichler, V. Zabolotnyy, H. Shiozawa, S. L. Molodtsov, D. Inosov, A. Koitzsch, M. Knupfer, J. Schiessling, et al., Phys. Rev. Lett. **100**, 037601 (2008).

[14] L. M. Malard, J. Nilsson, D. C. Elias, J. C. Brant, F. Plentz, E. S. Alves, A. H. Castro Neto, and M. A. Pimenta, Phys. Rev. B **76**, 201401 (2007).

[15] S. B. Trickey, F. Müller-Plathe, G. H. F. Diercksen, and J. C. Boettger, Phys. Rev. B **45**, 4460 (1992).

[16] S. Latil and L. Henrard, Phys. Rev. Lett. **97**, 036803 (2006).

[17] S. Latil, V. Meunier, and L. Henrard, Phys. Rev. B **76**, 201402 (2007).

[18] H. Min, B. Sahu, S. K. Banerjee, and A. H. MacDonald, Phys. Rev. B **75**, 155115 (2007).

[19] M. Aoki and H. Amawashi, Solid State Comm. **142**, 123 (2007).

[20] M. Orlita, C. Faugeras, G. Martinez, D. K. Maude, M. L. Sadowski, and M. Potemski, Phys. Rev. Lett. **100**, 136403 (2008).

[21] E. McCann, D. S. Abergel, and V. I. Falkoa, Solid State Comm. **143**, 110 (2007).

[22] J. Nilsson, A. H. Castro Neto, F. Guinea, and N. M. R. Peres, Phys. Rev. B **78**, 045405 (2008).

[23] E. McCann and V. I. Fal'ko, Phys. Rev. Lett. **96**, 086805 (2006).

[24] F. Guinea, A. H. Castro Neto, and N. M. R. Peres, Phys. Rev. B **73**, 245426 (2006).

[25] E. V. Castro, K. S. Novoselov, S. V. Morozov, N. M. R.

Peres, J. M. B. L. dos Santos, J. Nilsson, F. Guinea, A. K. Geim, and A. H. Castro Neto, Phys. Rev. Lett. **99**, 216802 (2007).
[26] J. B. Oostinga, H. B. Heersche, X. Liu, A. F. Morpurgo, and L. M. K. Vandersypen, Nat. Mat. **7**, 151 (2007).
[27] T. Ohta, A. Bostwick, T. Seyller, K. Horn, and E. Rotenberg, Sci. **313**, 951 (2006).
[28] Z. Q. Li, E. A. Henriksen, Z. Jiang, Z. Hao, M. C. Martin, P. Kim, H. L. Stormer, and D. N. Basov (2008), unpublished, arXiv:0807.3776.
[29] F. Wang, Y. Zhang, C. Tian, C. Girit, A. Zettl, M. Crommie, and Y. R. Shen, Sci. **320**, 206 (2008).
[30] A. B. Kuzmenko (2008), unpublished.
[31] D. S. L. Abergel and V. I. Fal'ko, Phys. Rev. B **75**, 155430 (2007).
[32] L. Benfatto, S. G. Sharapov, and J. P. Carbotte, Phys. Rev. B **77**, 125422 (2008).
[33] E. J. Nicol and J. P. Carbotte, Phys. Rev. B **77**, 155409 (2008).
[34] V. P. Gusynin, V. P. Sharapov, and J. P. Carbotte, Int. J. of Mod. Phys. B **21**, 4611 (2007).
[35] Another important source for the effective mass asymmetry is the in-plane next-nearest neighbor hopping[4] $\gamma_0' \sim 0.1\gamma_1$. However, it does not change the optical transition energies, and so has virtually no ffect on $\sigma(\Omega)$.
[36] E. McCann, Phys. Rev. B **74**, 161403 (2006).
[37] Z. Li, E. A. Henriksen, Z. Jiang, Z. Hao, M. C. Martin, P. Kim, H. Stormer, and D. N. Basov, Nat. Phys. **4**, 532 (2008), 1.4.4.
[38] Z. Q. Li, V. Podzorov, N. Sai, M. C. Martin, M. E. Gershenson, M. D. Ventra, and D. N. Basov, Phys. Rev. Lett. **99**, 016403 (2007).
[39] G. D. Mahan, *Many-Particle Physics* (Plenum, New York, 1990).
[40] J. Nilsson, private communication.
[41] A. H. R. Palser, Phys. Chem. Chem. Phys. **1**, 4459 (1999).
[42] A. N. Kolmogorov and V. H. Crespi, Phys. Rev. B **71**, 235415 (2005).
[43] J. D. Jackson, *Classical Electrodynamics* (Wiley, New York, 1998).
[44] D. S. L. Abergel, A. Russell, and V. I. Fal'ko, App. Phys. Lett. **91**, 063125 (2007).
[45] D. Abergel and V. I. Fal'ko, private communication.
[46] N. B. Brandt, S. M. Chudinov, and Y. G. Ponomarev, *Semimetals I: Graphite and its Compounds* (North-Holland, Amsterdam, 1988).
[47] W. W. Toy, M. S. Dresselhaus, and G. Dresselhaus, Phys. Rev. B **15**, 4077 (1977).
[48] D. Chung, J. of Mat. Sci. **37**, 1475 (2002).
[49] M. S. Dresselhaus, G. Dresselhaus, and J. E. Fischer, Phys. Rev. B **15**, 3180 (1977).

The work at UCSD is supported by the NSF Grant No. DMR-0706654 L.M.Z. and M.M.F., DOE Grant No. DE-FG02-00ER45799 Z.Q.L. and D.N.B., and by the UCSD ASC L.M. Z.. The Advanced Light Source is supported by the Director, Office of Science, Office of Basic Energy Sciences under the DOE Contract No. DE-AC02-05CH11231.